Optimal Location of Optical Ground Stations to Serve LEO Spacecraft

Iñigo del Portillo*, Marc Sanchez, Bruce Cameron, Edward Crawley
Massachusetts Institute of Technology
77 Massachusetts Ave 33-409
Cambridge, MA 02139
{portillo, msnet, bcameron, crawley}@mit.edu

***Abstract*—Free space optical communications (FSO) are envisioned as a disruptive technology for space communications. Among its advantages, FSO will allow higher throughputs (in the order of tenths of Gbps, which represents an improvement of 10 to 100 times with respect to current RF technology), together with significant reductions in size, weight, and power. However, the main drawback of FSO when compared to RF is the reduced link availability due to outages caused by cloud coverage over the receiving ground stations. Site diversity has already been proven to be an effective mitigation technique against cloud outage for geostationary satellites, but its usefulness in the context of low Earth orbit satellites can be challenged by correlated cloud coverage among all visible ground stations. This consideration, along with trade-offs between minimal cloud probability, minimal latency and proximity to supporting infrastructure should all be taken into account when selecting locations for networks of ground stations.**

This paper presents a model to optimally determine the location of optical ground stations to serve LEO missions, considering the aforementioned trade-offs. First we describe the atmospheric, latency, and infrastructure models used to evaluate the goodness of a network. Second, we statistically characterize the orbits of the customer missions that the ground network will serve. Finally, we present two case studies: The first one selects the best stations among a group of existing assets (stations in the Near Earth Network, other governmental agencies, and commercial facilities from ground segment operators). The second one determines the optimal locations for the ground stations considering an unconstrained scenario in which facilities can be placed at any point on the Earths surface. For each of these scenarios, we report the availability, latency and cost of ground stations of the Pareto-optimal networks.

TABLE OF CONTENTS

1. INTRODUCTION

Motivation

The capabilities of earth observation (EO) sensors on board low Earth orbit (LEO) satellites has increased exponentially in the last years, reaching levels that exceed the capacity of current space-to-ground communications technologies. Scientific data, such as measurements by hyperspectral imagery sensors or high-resolution wide-swath (HRWS) synthetic aperture radar (SAR) systems, are produced at rates of several gigabits per second, which need to be transmitted back to the Earth by the satellite communications subsystem for further processing and analysis.

Current satellite downlink communication technology is based on the use of RF links between the EO-satellite and a ground station or a relay satellite orbiting in geostationary orbit (i.e., NASA's TDRSS or ESA's EDRS systems). These RF links operate at several hundreds of megabits per second, a rate insufficient to transmit the information produced by the new generation of EO payloads. These limitations of RF are due both to technological constraints and spectrum-licensing constraints.

In light of these facts, new disruptive technologies are needed to download these huge data volumes, the most prominent of which is free space optical communications (FSO). In FSO, information is transmitted using lasers instead of RF equipment. Among its advantages, FSO allows for higher throughputs (in the order of tenths of Gbps, which represents an improvement of 10 to 100 times with respect to current RF technology), together with significant reductions in communications payload size, weight, and power.

However, the main drawback of FSO is the reduced link availability due to outages caused by cloud coverage over the receiving ground stations. Site diversity (i.e., having multiple optical ground stations (OGS) in line of sight with the satellite at any point in time) has been proven to be an effective mitigation technique for geostationary satellites, [1], [2], [3], [4], but its usefulness in the context of low Earth orbit (LEO) satellites can be challenged by correlated cloud coverage among all visible ground stations. Optical ground station location for LEO systems must be chosen so that the data volume that a satellite can download is maximized. This implies that maximum coverage considerations, along with trade-offs between minimal cloud probability, minimal latency, and proximity to supporting infrastructure, should all be taken into account when selecting locations for networks of ground stations.

This paper presents a model to optimally determine the location of optical ground stations to serve LEO missions, considering the aforementioned trade-offs. First, we describe the atmospheric, latency, and infrastructure models used to evaluate the goodness of a network, as well as the datasets on which these models are based. Second, we statistically characterize the orbits of the customer missions that the ground network serves. Finally, we present two case studies: The first one selects the best stations among a group of

978-1-5090-1613-6/17/31.00

existing assets, including stations in NASA's Near Earth Network, other governmental agencies, and commercial facilities from ground segment operators. The second one determines the optimal locations for the ground stations considering an unconstrained scenario in which facilities can be placed at any point on the Earth's surface. For each of these scenarios, we report the availability, latency and cost of ground stations of the optimal networks. Results show that the mean cloud probability over each OGS is the main driver when determining the location of the OGSs, which results in locations in the $\pm 20^{\circ}$ to $\pm 40^{\circ}$ latitude band being the most attractive candidate sites, instead of traditionally polar-latitude sites.

Literature Review

The problem of optimal location for optical ground stations that serve space missions has been a common topic of research for the last decade. Poulenard et. al. [3] analyzed the optimal location for a network of optical feeders for a broadband geostatinary satellite, while Fuchs et. al. analyzed in [2] the optimal locations for a German, European and African-European network of OGSs that serve a single geostationary satellite. Furthermore, the Optical Link Group Study report [4] used the Lasercom Network Optimization Tool (LNOT) [7], to analyze architecture in six different scenarios (LEO, HEO, GEO, L1, L2 and Deep Space). Focusing on LEO scenarios, Lacoste et al. [8] examined the data volume that several satellites in LEO (flying in SSO orbits with altitudes between 700 and 800 km) would be able to download to a network of six OGSs located in Western Europe; In Takayama et. al. [9], one year of imagery from MTSAT was used to analyze six architectures with up to eight OGSs located in Japan. Finally, Giggenbach et al. [11] built their cloud dataset from the International Satellite Cloud Climatology Project (ISCCP) dataset [12] and used a simulation approach to analyze the network availability for an Earth observation LEO satellite.

This literature review highlights that, even though several studies have been carried out for scenarios in which satellites are in geostationary orbit, a limited amount work has been conducted in order to determine the optimal locations for the scenario in which satellites are in LEO orbits. Instead, most of the previous studies for the LEO scenario analyze single point designs in which the performance of a small number of OGSs networks is assessed. The main goal of this paper is to cover this research gap, exploring the design-space of candidate locations for OGSs and determine the locations and characteristics of the optimal sites.

Paper Structure

The remainder of this paper is organized as follows: Section 2 presents the models (namely the atmospheric model, the latency model, and the infrastructure model) used to assess the goodness of the networks. Section 4 introduces the optimization algorithms used to determine the optimal locations for the OGSs. Section 3 describes the scenarios considered in this study, focusing on the statistical characterization of the orbits of the EO satellites that the OGS network will serve. Section 5 presents the results of our analysis for two case studies: an scenario with a fixed number of candidate OGS, and an unconstrained scenario in which facilities can be placed in any point on the Earths surface. Lastly, Section 6 derives the conclusions from the research and outlines the future directions of research in this area.

2. PROBLEM FORMULATION

The objective of this paper is to determine the optimal locations for a network of OGSs that serve space-missions in LEO. In particular, we try to identify the sites that are Pareto-optimal with regard to the main network performance drivers. That is, we try to determine which sites appear with a higher frequency in the architectures in the Pareto-front of the resulting tradespace. The Pareto-front is defined as the set of architectures which are non-dominated (i.e., the architectures if none of the metrics can be improved without degrading some of the other metrics).

We consider three attributes of the network (i.e., the metrics) as the performance drivers:

- **Availability of the network**, defined as percentage of the orbit-time that a satellite can access an OGS to download the data stored.
- **Latency of the network**, understood as the interval between two consecutive successful contacts between the satellite and an OGS.
- **Cost**, defined as the construction and operation costs incurred to maintain operative the ground assets that form the network.

The rest of this section is devoted to a description of the models used to evaluate the performance of a particular network with respect to each of these three attributes. First, we present the atmospheric model that is the base to compute the availability and latency values, and then, we introduce the infrastructure model used to estimate the construction and operation costs for the network.

Atmospheric Model

To assess the availability and latency of a network of OGSs, we developed a stochastic weather generator that simulates the cloud coverage dynamics. A stochastic weather generator is a statistical model that aims to quickly simulate realistic random sequences of atmospheric variables, such as temperature, winds, precipitation, and cloud coverage [13]. Our stochastic weather generator accurately represents the statistics of the cloud coverage at a single site (i.e., the probability that the site is covered by clouds at any point in time), as well as the spatial and time correlations of two-site scenarios (i.e., the probability of two geographically close facilities having clouded skies at the same time, and the probability of having cloud intervals of a certain duration).

Note that even though the approach used in references [1] and [14] for GEO scenarios captures the spatial correlation between ground stations, it fails to capture the temporal correlation dimension of the cloud dynamics. As these studies model the channel using a Bernoulli distributed random process, they assume that the cloud probabilities at a given time are independent of the previous state of the channel (i.e., the channel is memoryless). Even though these temporal statistics do not play an important role when assessing the performance of a network that serves geostationary satellites, as the length of unavailability periods is not a main concern, they are crucial in LEO networks. Note that for satellites in GEO the number of OGS in line of sight (LOS) is very high, hence if an OGS has clouded skies, the satellite can easily handover the communication to another OGS. This is not the case for LEO satellites, as the number of OGS in LOS with the spacecraft at any point in time is very small (normally no more than two or three). Our stochastic weather generator models the temporal and spatial correlation dynamics using

Markov chains, in which states represent the cloudiness state of one or multiple ground stations, and the state-transition probabilities are adjusted to represent the temporal dynamics of the cloud-occurrence process. This model is similar in essence to the one proposed in [15], but expanded to capture the spatial correlation between OGSs in geographically close locations, and adjusted with empirical parameters obtained from cloud-coverage satellite imagery to capture the temporal dimension of the cloud-occurrence stochastic process.

Spatially-isolated ground station model—First, we describe the Markov chain that models a single, spatially-isolated OGS with cloud probability θ_c. In this work we assume that θ_c can be modeled as a step function (i.e., a piecewise constant function) with interval length equal to one month. As the ground station is isolated from any other OGS, we can model it's channel state using a Markov chain with two states, CLEAR skies and CLOUDS, as shown in Figure 1. This two-state Markov chain is also referred as the Gilbert-Elliot model [16].

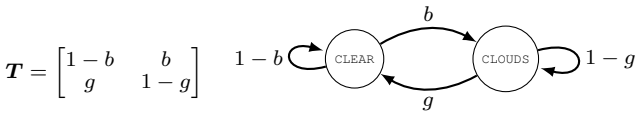

Figure 1: **Gilbert-Elliot model implemented in the stochastic weather generator for a single and spatially-isolated ground station.**

The stationary probabilities of each state (π_G for CLEAR and π_B for CLOUDS) are a function of g and b, the transition probabilities from state CLOUDS to CLEAR and form state CLEAR to CLOUDS respectively, as shown in Eq. 1.

$$\pi_G = \frac{g}{g+b} = (1-\theta_c) \qquad \pi_B = \frac{b}{g+b} = \theta_c \tag{1}$$

Note that once that we fix the value of θ_c, the Gilbert-Elliot model has one remaining degree of freedom, the value of g (or b). In particular, parameter g controls the sojourn time of the CLOUDS state (i.e., the expected duration of a clouds interval, or analogously the average time that the system will remain in state CLOUDS before transitioning to state CLEAR). Equation 2 shows the value of the sojourn time for both states as a function of the transition probabilities g and b.

$$E[\texttt{CLOUDS}] = \frac{T}{g} \qquad E[\texttt{CLEAR}] = \frac{T}{b} = \frac{T}{g}\frac{\theta_c}{(1-\theta_c)} \tag{2}$$

where T is the time-step (in units of time) between consecutive samples drawn from the Markov chain. T is also the time-step value chosen for the stochastic weather generator, and must be selected so that a compromise between simulation fidelity and computational effort is attained. For our analysis, we use a value of 15 minutes.

In order to complete the parametrization of the single and spatially-isolated site, we experimentally determine the average duration of the cloud intervals, $E[\texttt{CLOUDS}]$, using 2-hour frequency satellite imagery data captured by EUMETSAT during the years 2005, 2006, 2010, and 2011. Figure 2 shows the mean duration of the cloud-interval vs. the monthly cloud probability for 66 ground stations located in Europe and Africa. The complete list of ground stations can be found in the Annex of reference [2].

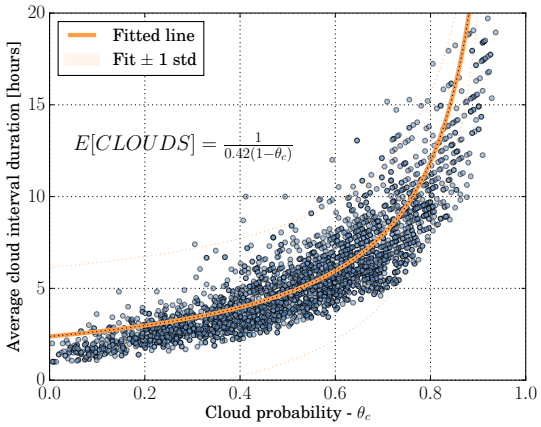

Figure 2: **Average cloud interval duration vs. monthly cloud probability during the years 2005,2006,2010, and 2011 for 66 ground stations in Europe**

Figure 2 shows that the average cloud interval duration is inversely proportional to the cloud probability. We fitted the hyperbolic curve that minimizes the RMSE, and obtained that the value for $E[\texttt{CLOUDS}]$, in hours, can be modeled as:

$$E[\texttt{CLOUDS}] = \frac{1}{0.42(1-\theta_c)}. \tag{3}$$

Using this equation together with Eq. 2, and the fact that $T = 15$ minutes (or 0.25 hours), we end up with the following expressions for b and g:

$$g = 0.42 \cdot T(1-\theta_c) \qquad b = 0.42 \cdot T\theta_c \tag{4}$$

Finally, we proceed to validate our two-state Markov model for a single, isolated OGS by computing the mean relative errors for the mean and the variance of the cloud interval duration for the 66 OGS, as well as the value of several statistical distances that quantify the resemblance between two PDFs (the real PDF derived from the 2-hour frequency satellite imagery data, and the PDF obtained by sampling the Markov chain). In particular, we compare the Gilbert-Elliot model we just presented, to a Bernoulli-Process model (the cloud dynamics are assumed to follow a Bernoulli process of mean θ_c), and to the Gamma-dist and Beta-dist models (models that use a Gamma-distribution and a Beta-distribution which were fitted to the empirical sequence, computed using satellite imagery, of cloud interval durations). The Gamma-dist model was proposed in [17], whereas Beta-dist model was proposed in [18]. The results are shown in Table 1.

Table 1: **Comparison of the performance of different statistical models for the cloud interval duration.**

	Gilbert Elliot	Bernoulli Process	Gamma-dist. (adjusted)	Beta-dist. (adjusted)
# Params	θ_c	θ_c	2	2
Err in mean (%)	23.56	65.60	275.99	61.04
Err in std (%)	38.56	172.1	480.94	169.66

Note that the proposed Gilbert-Elliot model only requires knowledge of one parameter of the OGS, the cloud probability, which can be obtained from multiple datasets at different time scales (daily, monthly, and yearly cloud probabilities).

Despite the simplicity of the model, its performance is acceptable for a first order approximation of the cloud dynamics (i.e., the model has no relative error in the mean and variance of the cloud probability, and the mean relative errors for the mean and standard deviation of the cloud intervals duration is below 25% and 40% respectively).

Two spatially-correlated ground stations model—Next, we describe the Markov chain model for a pair of spatially correlated ground stations. We model this situation using a 4-state Markov chain, as shown in Figure 3. To simplify the model, we assume that only one of the ground stations can change it's state (from CLEAR to CLOUDS or vice-versa) at each transition in the Markov chain.

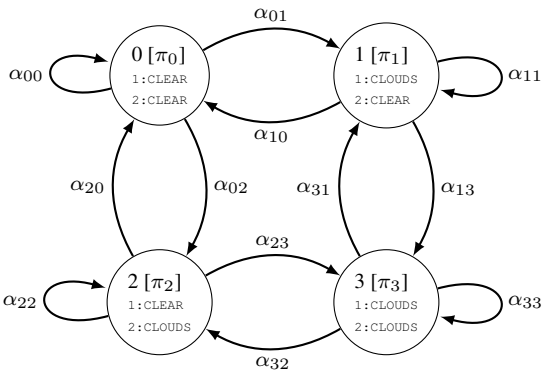

$$\boldsymbol{P} = \begin{bmatrix} \alpha_{00} & \alpha_{01} & \alpha_{02} & 0 \\ \alpha_{10} & \alpha_{11} & 0 & \alpha_{13} \\ \alpha_{20} & 0 & \alpha_{22} & \alpha_{23} \\ 0 & \alpha_{31} & \alpha_{32} & \alpha_{33} \end{bmatrix} \qquad \Pi = \begin{bmatrix} \pi_0 \\ \pi_1 \\ \pi_2 \\ \pi_3 \end{bmatrix} \quad (5)$$

Figure 3: **Gilbert-Elliot model implemented in the stochastic weather generator for two spatially-correlated sites.**

Let $\{\pi_0, \pi_1, \pi_2, \pi_3\}$ be the stationary state-probabilities, P be the transition probabilities matrix of the system (as shown in Eq. 5), and $\theta_c^{(1)}$ and $\theta_c^{(2)}$ be the cloud probabilities at each OGS, then, it must be satisfied that

$$\pi_1 + \pi_3 = \theta_c^{(1)} \qquad \pi_2 + \pi_3 = \theta_c^{(2)}, \quad (6)$$

and analogously,

$$\pi_0 + \pi_1 = (1 - \theta_c^{(1)}) \qquad \pi_0 + \pi_2 = (1 - \theta_c^{(2)}). \quad (7)$$

If the correlation coefficient between the ground stations is ρ, then it must also be satisfied that

$$\begin{aligned} \rho &= \frac{E[\chi^{(1)}\chi^{(2)}] - E[\chi^{(1)}]E[\chi^{(2)}]}{\text{var}(\chi^{(1)})\text{var}(\chi^{(2)})} \\ &= \frac{E[\chi^{(1)}\chi^{(2)}] - \theta_c^{(1)}\theta_c^{(2)}}{\theta_c^{(1)}(1-\theta_c^{(1)})\theta_c^{(2)}(1-\theta_c^{(2)})} \\ &= \frac{\pi_0\pi_3 - \pi_1\pi_2}{(\pi_0+\pi_1)(\pi_0+\pi_2)(\pi_1+\pi_3)(\pi_2+\pi_3)}, \end{aligned} \quad (8)$$

where $\chi^{(1)}$ ($\chi^{(2)}$) is the binary random variable that indicates whether the skies over the first (second) OGS are covered by clouds or not, $E[\chi^{(1)}]$ is its mean, and $\text{var}(\chi^{(1)})$ its variance.

Solving the 4-equations 4-unknowns system composed by Eqs. 7, Eq. 8, and $\pi_0 + \pi_1 + \pi_2 + \pi_3 = 1$, we obtain the stationary state-probabilities of the system as:

$$\pi_0 = (1-\theta_c^{(1)})(1-\theta_c^{(2)})(\rho\theta_c^{(1)}\theta_c^{(2)} + 1) \quad (9)$$

$$\pi_1 = \theta_c^{(1)}\left(1-\theta_c^{(2)}\right)\left(1-\rho\theta_c^{(2)}(1-\theta_c^{(1)})\right) \quad (10)$$

$$\pi_2 = \theta_c^{(2)}\left(1-\theta_c^{(1)}\right)\left(1-\rho\theta_c^{(1)}(1-\theta_c^{2})\right) \quad (11)$$

$$\pi_3 = \theta_c^{(1)}\theta_c^{(2)}\left(\rho\theta_c^{(1)}\theta_c^{(2)} - \rho\theta_c^{(1)} - \rho\theta_c^{(2)} + \rho + 1\right) \quad (12)$$

Once that the stationary state-probabilities π_i have been determined, the transition probabilities are computed by solving the system of equations formed by Eqs. 13 - 17 below:

$$\boldsymbol{P}\,\underline{\mathbf{1}} = \underline{\mathbf{1}} \;\rightarrow\; \sum_{j=0}^{3}\alpha_{ij} = 1, \quad \forall i = 0,1,2,3 \quad (13)$$

$$\boldsymbol{P}\,\boldsymbol{\Pi} = \boldsymbol{\Pi} \;\rightarrow\; \sum_{j=0}^{3}\pi_j\alpha_{ij} = \pi_i, \quad \forall i = 0,1,2,3 \quad (14)$$

$$E[\texttt{CLOUDS}^{(1)}] = \frac{T}{g_1} \qquad E[\texttt{CLOUDS}^{(2)}] = \frac{T}{g_2} \quad (15)$$

$$E[\texttt{STATE}_3] = T\left(1 - \frac{1}{\alpha_{33}}\right) \quad (16)$$

$$E[\texttt{STATE}_0] = T\left(1 - \frac{1}{\alpha_{00}}\right) \quad (17)$$

where Eq. 13 shows that the sum of the elements in a row of the transition probabilities matrix P must add up to 1, and Eq. 14 shows that the stationary state-probabilities of the system must be equal to the values previously derived for $\{\pi_0, \pi_1, \pi_2, \pi_3\}$. Equations 15-17 determine the sojourn times for the states $\texttt{CLOUDS}^{(x)}$ (expected times of cloud intervals in ground station $x, x \in [1,2]$, $\texttt{STATE}_3$ (both stations have clouds simultaneously), and $\texttt{STATE}_0$ (none of the stations have clouds simultaneously). The exact expressions for the sojourn times of the CLOUD states for each OGS can be found using the formulas proposed by Rubino and Sericola in [19], which we reproduce for the particular Markov chain under consideration,

$$v_1^{(x)} = \Pi_B^{(x)} + \Pi_{B_c}^{(x)}(I - P_{B_c}^{(x)})^{-1}P_{BB_c}^{(x)} \quad (18)$$

$$E[\texttt{CLOUDS}^{(x)}] = v_1^{(x)}(I - P_B^{(x)})^{-1}1^T \quad (19)$$

where the superscript $^{(x)}$ makes reference to the index of corresponding ground station ($x \in [1,2]$). The values for the matrices $P_{B_c}^{(x)}$, $P_B^{(x)}$, and $P_{BB_c}^{(x)}$, as well as for the vectors $\Pi_B^{(x)}$, $\Pi_{B_c}^{(x)}$ for ground station 1 can be found in Eq. 20 and for ground station 2 in Eq. 21.

$$P_B^{(1)} = \begin{bmatrix} \alpha_{11} & \alpha_{13} \\ \alpha_{31} & \alpha_{33} \end{bmatrix} \quad P_{B_c}^{(1)} = \begin{bmatrix} \alpha_{00} & \alpha_{02} \\ \alpha_{20} & \alpha_{22} \end{bmatrix} \quad P_{BB_c}^{(1)} = \begin{bmatrix} \alpha_{10} & 0 \\ 0 & \alpha_{32} \end{bmatrix}$$

$$\Pi_B^{(1)} = [\pi_1 \quad \pi_3] \qquad \Pi_{B_c}^{(1)} = [\pi_0 \quad \pi_2] \quad (20)$$

$$P_B^{(2)} = \begin{bmatrix} \alpha_{22} & \alpha_{23} \\ \alpha_{32} & \alpha_{33} \end{bmatrix} \quad P_{B_c}^{(2)} = \begin{bmatrix} \alpha_{00} & \alpha_{01} \\ \alpha_{10} & \alpha_{22} \end{bmatrix} \quad P_{BB_c}^{(2)} = \begin{bmatrix} \alpha_{20} & 0 \\ 0 & \alpha_{31} \end{bmatrix}$$

$$\Pi_B^{(2)} = [\pi_2 \quad \pi_3] \qquad \Pi_{B_c}^{(2)} = [\pi_0 \quad \pi_1] \quad (21)$$

This system of 12-equations with 12-unknowns (Eqs. 13-17) can be solved numerically using any symbolic manipulation package. Given the complexity of the expressions for $E[\texttt{CLOUDS}^{(1)}]$, and $E[\texttt{CLOUDS}^{(2)}]$, we were not able to find closed expressions for the α_{ij} variables.

Note that in order to build this model, 3 parameters are necessary. First, we need the cloud probabilities of both ground stations, $\theta_c^{(1)}, \theta_c^{(2)}$. This values are obtained form the MODIS dataset [20]. Second, the spatial-correlation coefficient, ρ, is needed, which is computed using the model proposed in [21] (See Eq. 23, in which d is the distance between the two correlated ground stations (in km.)). Finally, the value of the mean durations of the cloud intervals for each OGS is required. These values, equivalent to the sojourn times previously described, are computed using Eq. 4 for single ground stations ($E[\texttt{CLOUDS}^{(x)}],\ x = 1, 2$), and for the other states ($E[\texttt{STATE}_x],\ x = 0, 3$) we propose the use of Eq. 22. Note that all the sojourn values are computed from $\theta_c^{(1)}, \theta_c^{(2)}$, ρ, and the stationary probabilities of the Markov chain (which in turn are computed from $\theta_c^{(1)}, \theta_c^{(2)}, \rho$).

$$E[\texttt{STATE}_x] = 0.21T(1 - \pi_3) \tag{22}$$

$$\rho_{ij} = \exp\left(\frac{-d}{300}\right), \qquad \text{d in km.} \tag{23}$$

Availability and Latency Models

We define the availability of the network as the fraction of time of a satellite orbit in which the satellite can establish contact with a ground station. For example, the availability for a satellite in GEO that uses RF communications is close to 100 %, as there is a ground station in line of sight with the spacecraft continuously. That being said, the actual experienced availability can be lower due to malfunctioning of the communications subsystems on board of the spacecraft or on the ground, scheduled maintenance operations, or other operational reasons, but in this study we will ignore the effect of these situations. For satellites in LEO, however, this value is much lower, since during most part of the orbit the spacecraft is not in line of sight with any ground station.

To compute the availability and the latency of a network of ground station, and given the orbits of the LEO spacecraft that will be served by the network (see Section 3), we use the following 5-step procedure (illustrated in Fig. 4).

First, using the same method as described in [14], we compute for each ground station (OGS_i) a visibility mask (M_{gs}^i) that indicates which points at a given height (h) will be in line of sight with the ground station. This mask corresponds to the set of points for which the elevation angle is above the minimum elevation angle (ϵ_{min}) admissible at the receiver ground station. The elevation angle between a point (P) at height h and the OGS is computed using Eq. 25, 26

$$M_{gs}^i = \{P = (L_P, l_P) \quad | \quad \epsilon(P) > \epsilon_{min}\} \tag{24}$$

$$\epsilon(P) = \arccos \frac{sin\gamma}{\sqrt{1 + \frac{R_E}{R_E+h}^2 - 2\frac{R_E}{R_E+h}\cos\gamma}} \tag{25}$$

$$\begin{aligned}\cos(\gamma) = {} & \sin L_P \sin L_{OGS} + \\ & + \cos L_P \cos L_{OGS} \cos(l_P - l_{OGS})\end{aligned} \tag{26}$$

where L_{OGS} and l_{OGS} are respectively the latitude and longitude coordinates of the OGS, L_P and l_P are the latitude and longitude coordinates of the point P.

Second, for every month between June 2005 and June 2015, we generate an N_s-samples sequence of cloud occurrences using the stochastic weather generator described in Section 2 (for the analyses presented in this paper, $N_s = 10,000$, equivalent to 104 days). The monthly cloud fraction $\theta_{c_m}^i$ at each ground station location is estimated from the MODIS dataset [20].

Third, we compute for each user and every point of its orbit, the intervals in which it is in LOS with an OGS, using the visibility masks (M_{GS}^i) computed in the first step. Combining this data with the weather state as denoted by the cloud sequence generated in Step 1, we determine the sets of intervals in which a) the user is in LOS with at least one OGS and the weather conditions permits the establishment of a successful link with at least one OGS, b) the user is in LOS with at least one OGS but clouds make it impossible to establish a link with any of the OGSs, and c) the user is not in LOS with any OGS.

Fourth, the total monthly time in which a link can be established by the user and the ground station and the duration of the intervals between successive contacts (latency) are computed using these intervals. In particular, the network availability for month m, (NA_m), is defined as

$$\text{NA}_m = 100 \cdot \sum_n \frac{d_n^C}{N_s \cdot T}, \tag{27}$$

where d_n^C is the duration of contact n, and T is the sampling time (in our study 15 minutes). The monthly latency lat_m is defined as the percentile 95% value on the CDF of latency times (i.e., the 95% of the cumulative distribution function of the duration of intervals between consecutive contacts).

Finally, we aggregate the monthly availabilities and the monthly latencies to an overall network metric. The **optical network availability** (ONA), is computed as the percentile 5% of the monthly availabilities

$$\text{ONA} = \text{Perc}_5\left[\text{NA}_m\right], \tag{28}$$

and the **latency** of the network (lat), as the percentile 95% of the monthly latencies:

$$\text{lat} = \text{Perc}_{95}\left[\text{lat}_m\right]. \tag{29}$$

These two metrics are interpreted as follows. Optical network availability establishes that for 95% of the months network availability is higher or equal than the ONA. The minimum data-volume that can be downloaded 95% of the months is computed by simply multiplying the ONA by the data rate of the optical transmitter on-board the spacecraft. The latency value establishes that for 95% of the months, the user is having a contact in a time less or equal than the latency value for 95% of it's orbits.

Infrastructure Model

The goal of the infrastructure model is to provide an estimation of the lifecycle cost of a network that is good enough for relative comparison across architectures. This model assumes that the cost of an architecture is the sum of the costs of each

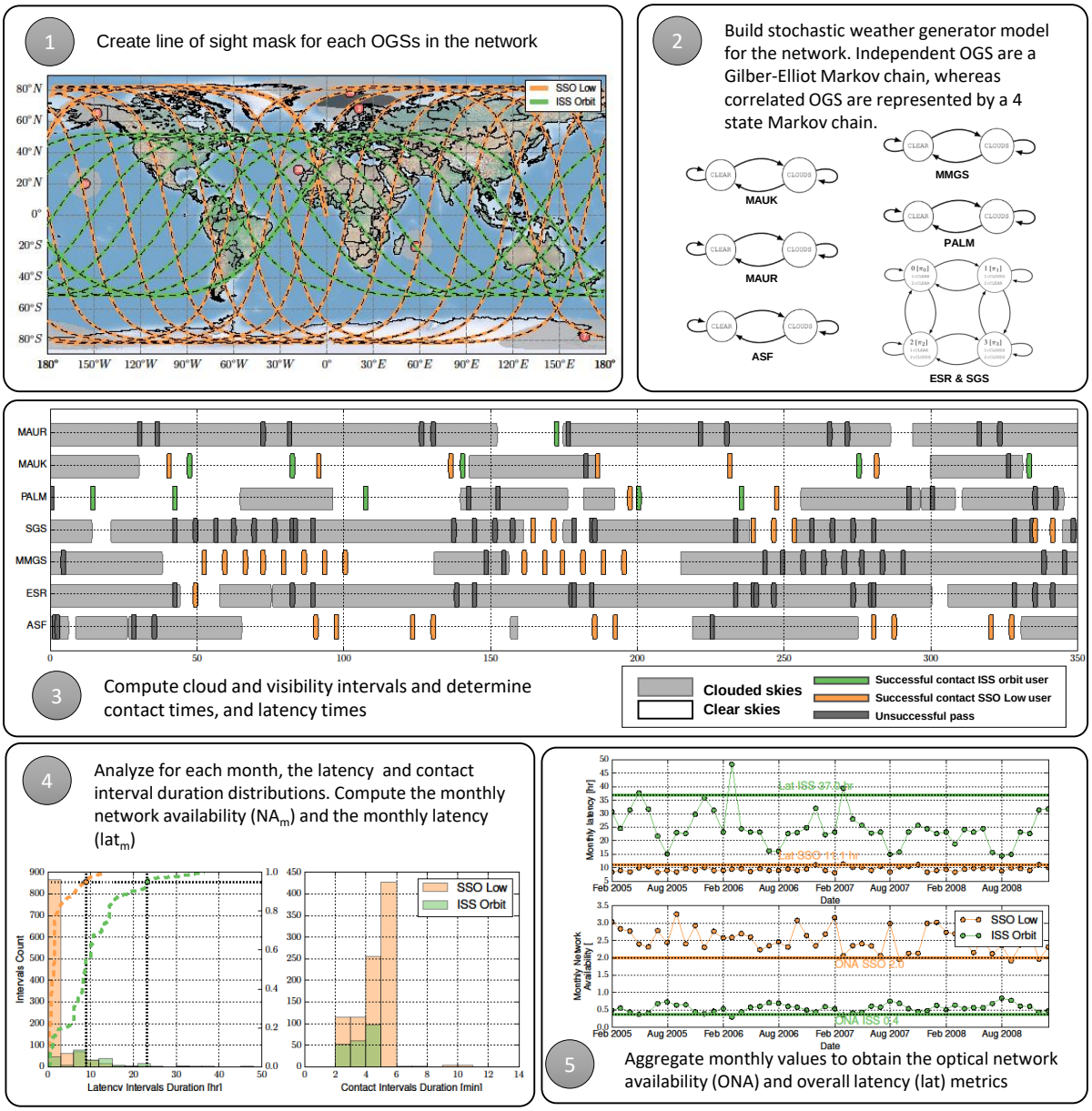

Figure 4: **Procedure to compute the latency and availability. In this example, a network with 7 OGSs is evaluated. Step 1 shows the LOS mask of the OGSs with two customers (*ISS orbit* and *SSO Low orbit*). Step 2 shows the corresponding Markov model for the stochastic weather generator. Step 3 shows the cloud intervals, as well as the contact opportunities. Step 4 shows the statistics of the latency and contact duration for the month of June 2009. Step 5 shows the time series of monthly network availabilities and latencies and the values of the overall network metrics.**

of the OGSs that compose it. The model employed is similar to the one used in [14]. The main components of the non-recurring and recurring costs that compose this model are summarized.

Non-recurring costs—The non-recurring costs drivers of each ground station are site construction, optical terminal cost, and wide area communication network (WAN) development. These costs are only incurred once, when the ground station is built. The cost of the telescope is computed using a parametric model similar to the one presented in [22], [23], the construction cost is computed using a parametric model given in the DoD facilities pricing guide [24], and the WAN development cost is computed using a CER that relates the cost of the optical fiber with the distance to the closest Internet exchange point (IXP). The total cost is

$$C_{nr} = F(L)(C_{WAN,nr} + C_{cons} + C_{tels}), \tag{30}$$

where F(L) is the cost area factor for a ground station located in country L. The exact equations for $C_{WAN,nr}$, C_{cons}, and C_{tels} can be found in reference [14].

Recurring costs—The recurring costs of the model account for operations and maintenance costs associated to each ground station. The recurring cost of an OGS is computed as the sum of three components: employees salary, operational costs of the WAN and maintenance and operational cost of the facility and the telescope. The recurring costs are

$$C_r = \sum_{t=1}^{T} \frac{C_{salary} + C_{\text{WAN},r} + C_{M\&O}}{(1 + I(r))^t}, \tag{31}$$

where C_{salary} are the salary costs, $C_{\text{WAN},r}$ are the yearly fees of the WAN network, $C_{M\&O}$ are the costs of maintenance and operations, $I(r)$ is the inflation factor, T is the lifetime of the ground stations (set to 15 years in our analysis) and t is an index that designates the difference between the year in which we are accounting the recurring costs and the initial year (2015). The equations, to compute C_{salary}, $C_{\text{WAN},r}$, $C_{M\&O}$ together with the rationale behind them, can be found in reference [14].

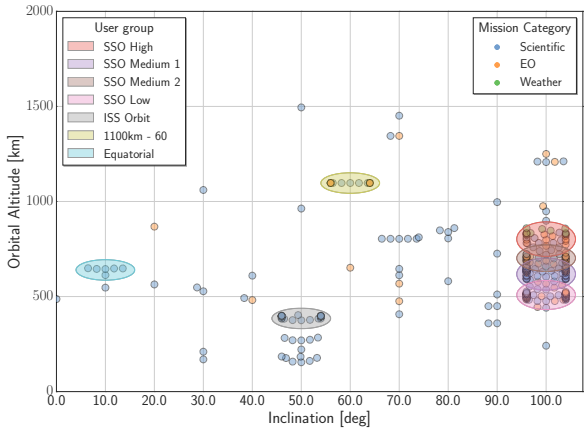

Figure 5: **LEO satellites with scientific, weather or Earth observation mission orbital distribution. (Note, the inclination of the satellites has been slightly modified in order to avoid overlapping of close satellites.)**

3. SCENARIO DESCRIPTION

Orbital characteristics of the user base

When designing a network of optical ground stations to serve LEO missions, the statistical characteristics of the user base that the network will serve need to be defined. These statistics are the driving requirement for the locations of the OGSs. For example, if the network will mainly support spacecraft in sun-synchronous orbits (SSO), having ground stations in the polar regions is an appealing options, as these facilities guarantee one pass per orbit. However, if the user base is mostly composed of spacecraft with inclinations below 60 degrees, these grounds stations will not provide any benefit, as no passes will occur between the satellite and the high-latitude ground stations.

To characterize the statistics of the mission that the network serves, the following hypotheses were assumed:

- The statistical composition of the user base (in terms of distribution of orbital inclinations and orbital altitudes) in the future is similar to the current statistics of operations satellites.
- The OGS network is only serves missions in LEO with scientific, Earth observation, and weather monitoring purposes.
- Only LEO satellites with an orbital altitude below 2000 km we considered.

We used AGI STK's [25] Standard Object Database, (which in turn contains data from the U.S. Strategic Command (USSTRATCOM) 12,000 space objects TLEs database), to determine the current active satellites that satisfy the previous hypothesis. 211 records of operational scientific satellites, 9 records of operational weather satellites, and 111 records of operational Earth observation satellites were used for the analysis. The complete record of satellites can be accessed at the project webpage[2].

[2]Project webpage: `http://www.mit.edu/~portillo/projects/LEO_coverage`

Figure 5 shows a scatter-plot of the altitude (y-axis) and orbital inclination (x-axis) of the satellites. Big clusters of satellites dominate the satellite population. Most of the satellites are located in SSO orbits at different heights. Four groups can be distinguished in this region; the high altitude orbits ($\approx$ 800 km) is occupied by a group of 33 weather and EO satellites; at a lower altitude ($\approx$ 700 km) another 39 scientific satellites can be found; the 600 km orbits hosts a group of 62 satellites; and finally, at the lower SSO altitudes ($\approx$ 507 km) 64 scientific and EO satellites orbit the Earth. In addition, a considerable number of satellites are located on the ISS orbit (33 satellites, mostly cubesats deployed from the international station), the 1100 km - 60 degrees orbit (15 satellites of the Yaogan constellation), and an almost equatorial orbit (6 scientific satellites).

The satellites that fall in these 7 groups represent 80 % of the current scientific, Earth observation and weather satellites. In the subsequent analyses, the user-base composition has same statistics as those described in this section. For that purpose, a weight proportional to the number of satellites that fall on each group is assigned to the group. Table 2 summarizes the group characteristics.

Candidate locations for the optical ground stations

The criteria to select the candidate locations considered on each of the two analyses conducted follows. The first analysis determines the Pareto-optimal subsets of OGSs given a candidate set of existing facilities. The second analysis considers an unconstrained scenario in which any point in a certain set of countries is considered as a potential candidate location for an OGSs.

Candidate locations for the fixed candidate set scenario—For the first scenario, the candidate set of ground stations was determined using the following criteria:

- Current RF ground station locations belonging to one of the space governmental agencies (NASA, ESA)
- Current locations owned by commercial service providers such as (SSC, KSAT)
- The list of Astronomical observatories proposed in reference [4].

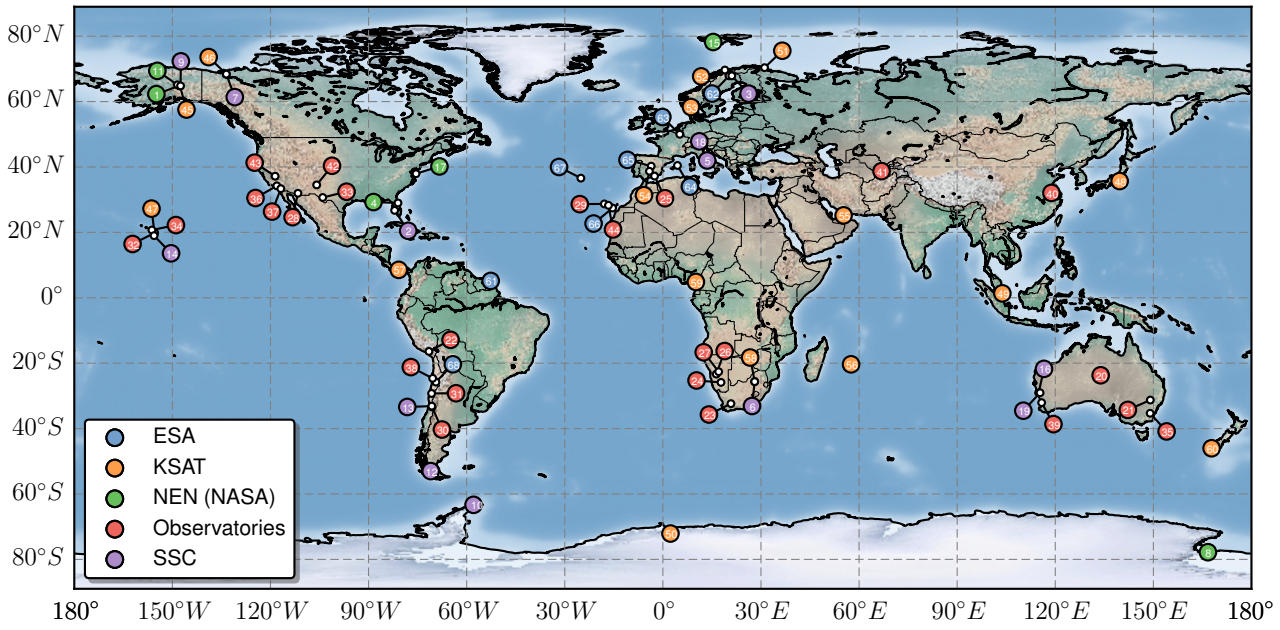

Figure 6: **Candidate locations on the fixed scenario. More information for each location can be found in Table 4.**

Table 2: **Characteristic of the user-base considered for the analyses**

ID	Name	Inc [deg]	Alt [km]	Inc min [deg]	Inc max [deg]	Alt. min [km]	Alt. max [km]	Comments	# Sat. #	Weight [%]
1	SSO High	98.5	802	98.41	98.72	758	859	All weather satellites, and several EO satellites	33	13.10
2	SSO Medium 1	97.87	617	97.37	98.37	553	647	Similar number of scientific and EO satellites	62	24.60
3	SSO Medium 2	97.9	702	97.67	98.3	665	743	Mostly scientific satellites	39	15.48
4	SSO Low	97.5	508	97.2	98.2	475	560	Similar number of Scientific and EO satellites	64	25.40
5	ISS Orbit	51.64	385	51.63	51.64	375	402	A large number of cubesats deployed from the ISS	33	13.10
6	1100 km -60	63.4	1097	63.37	63.41	1097	1097	Composed by the Yaogan constellation	15	5.95
7	Equatorial	6.0	640	5.99	6.02	613	649	Scientific satellites (LEMUR, Nustar, ASTROSAT)	6	2.38

The list of candidate locations comprises a total of 68 ground stations. Figure 6 shows a world map with the location of each of the ground stations. Table 4 contains extra information regarding the ground station locations.

Candidate locations for the unconstrained scenario— For the second analysis, every land-point on the Earth with the exception of a set of countries that do not have political stability was considered. The countries discarded correspond to the 20% lowest scoring countries in the *Political Stability and Absence of Violence/Terrorism index* from the Worldwide Governance Indicators dataset of the WorldBank [26]. For instance, countries located in Saharan Africa, south-west Asia, as well as Russia, Colombia and Venezuela are excluded from the analysis. The full list of banned countries can be found in [27].

4. Optimization Algorithms

To determine the optimal locations for the OGSs, we used one of two optimization algorithms, depending on the scenario under analysis: for the fixed candidate set scenario, the Non-dominated Sorting Genetic Algorithm-II (NSGA-II), an efficient multi-objective genetic algorithm, was selected; for the unconstrained scenario, a variable-length chromosome genetic algorithm (VLC-GA) was selected. The most relevant characteristics of both algorithms are stated; more information regarding the algorithms and its implementation can be found in references , [27], [28] for NSGA-II, and in [27], [29] for VLC-GA.

Fixed candidate set scenario: NSGA-II

NSGA-II operates as follows: Initially, a random population of N architectures (populated using random subsets of OGSs) is generated and its performance (availability, latency and cost) is evaluated. Next, $\frac{N}{2}$ architectures are selected to act as parents for the following generation using the following

criteria [28]:

- Architectures with lower Pareto ranking are selected first.
- Among architectures with similar Pareto ranking those with lower crowding distance are selected first.

Then, two genetic operators, *crossover* and *mutation*, are applied over the parent-architectures to produce a new generation. Crossover takes as inputs two parents and produces two offspring. Every ground station present in each parent is assigned to one of their offspring with equal probability (i.e., we use uniform crossover [30] over the OGSs on each parent). In total, $\frac{N}{2}$ offspring are produced from the $\frac{N}{2}$ parents, for a total of N architectures that form a new generation. Mutation removes an OGS from an architecture with probability p_{remove}, and adds a new OGS with probability p_{add}. The mutation operator is applied with probability p_{mut} to all the architectures in a generation.

Applying both operators results in a new generation of N architectures that need to be evaluated again. The process repeats until a termination criterion (i.e. maximum number of generations G_{max} evaluated, no new architectures in the Pareto Front) is met.

Unconstrained scenario: VLC-GA

A VLC-GA is a genetic algorithm in which the finesse of the solution depends on the length of the chromosome. This idea of progressive refinement of the solution suits the unconstrained scenario optimization problem well; first, coarse regions that contain good locations are identified, and then, the extent of these regions is refined in subsequent steps. The process is as follows:

1. Divide the world into square regions and delete the ones that do not contain any valid points (all-water regions, regions inside banned countries). The length of the chromosome is then equal to the number of regions.
2. Sample N architectures randomly with OGS inside the regions defined in Step 1, and evaluate them.
3. For each region, compute the average Pareto-ranking of the architecture with at least one OGS in that region.
4. Sub-divide the top-scoring regions (increasing the finesse) and merge pairs of adjacent regions that score poorly in the Pareto-ranking metric. The chromosome length is updated and equals the new number of regions.
5. Apply the crossover and mutation genetic operators (similar to those described in the previous subsection).
6. Iterate through steps 3-5 until the termination criteria is met.

5. RESULTS

Fixed candidate set scenario

In this analysis, we look for the optimal subset of OGSs given a candidate set of stations (i.e., the ground stations described in Table 4). Assuming that the user base is similar to the one described in Table 2, NA_m and lat_m values are computed for every month between January 2005 and December 2008 using the procedure described in Section 2. The monthly cloud probabilities for each OGS are extracted from the MODIS dataset [20]. The cost of each architecture is estimated using the infrastructure model presented in Section 2, assuming a 15 year lifecycle. We configure our GA with the following set up of parameters: $N = 10,000$, $G_{max} = 20$, $p_{mut} = 0.3$, $p_{add} = p_{remove} = 0.5$. Finally, we introduce an additional constraint to limit the stretch of the design-space: the number of OGSs on any given architecture is limited to a minimum of 3 and a maximum of 20.

Figure 8 shows the resulting tradespace for this analysis. Each marker corresponds to an architecture, and those encircled in red represent the architectures in the Pareto-front (Pareto-index equal to 1). The maximum ONA value attained by any architecture is 7.97%, whereas the minimum latency is 3 hours and 55 minutes. We observe that the improvements in latency obtained by increasing the lifecycle cost (i.e., adding more OGSs or selecting more expensive locations) is almost negligible for costs higher than $750M. However, for the ONA, availability can be increased beyond the 7.97% obtained by adding extra OGSs and increasing the cost of the architecture.

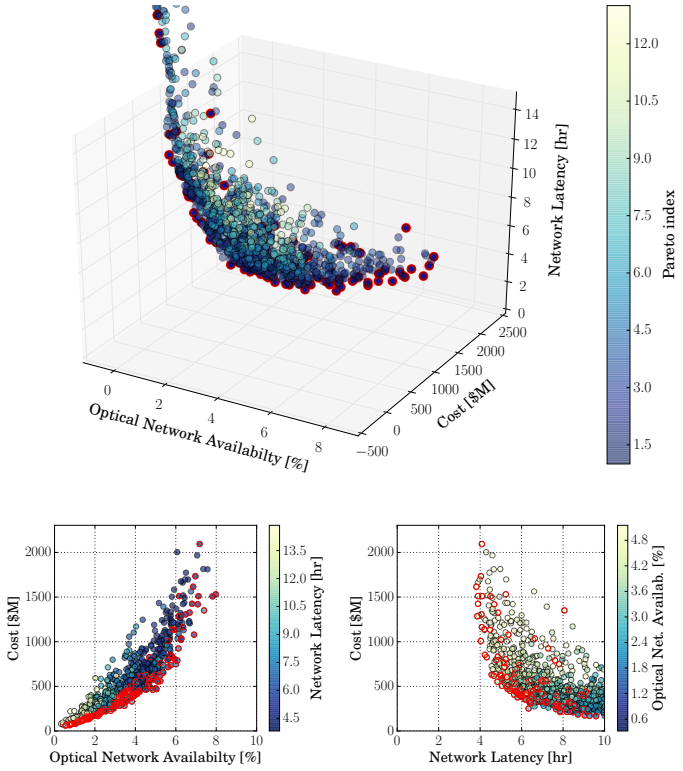

Figure 8: **Tradespace results for the fixed candidate set scenario. Each marker represents an architecture. The metric-space is represented in the top graph, whereas projections of this space in the ONA-cost (left) and latency-cost (right) are represented in the bottom views. Architectures in the Pareto-front are marked in red.**

Figure 9 shows the popularity of each OGS within the architectures that belong to the metric-space Pareto-front, while Figure 7 shows the same information geographically over a world map.The popularity of an OGS is measured by computing the frequency in which it appears in networks that belong to the Pareto-front. The most striking result to emerge from this analysis is that popular ground stations are no longer located in polar latitudes (with the exception of Inuvik in Canada), even though almost 80 % of the user-base is composed of SSO satellites. This is a major difference compared to current architectures for networks that

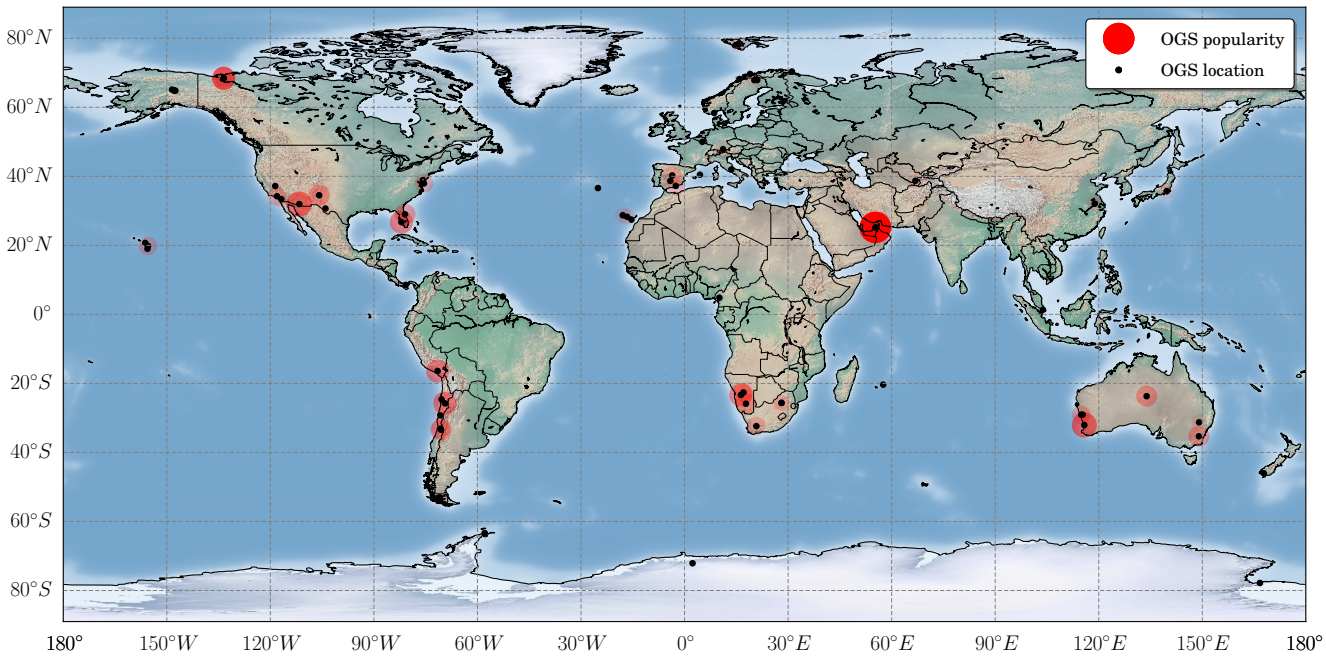

Figure 7: **World-map view of the popularity of the OGSs for the fixed candidate set scenario. The size and intensity of each circle is proportional to the percentage of occurrence of that OGS across the Pareto-front architectures**

serve LEO satellites, where polar ground stations are one of the most valuable assets (since they guarantee one pass per orbit). Instead, our study reveals that locations like Dubai, the south of the United States, the astronomical observatories at The Andes, the facilities in Namibia, and those in western Australia, are the most popular sites for the location of OGSs that serve LEO missions.

The reason for this is that OGSs located close to polar latitudes present a very high cloud probability, and therefore contribute very little to increase the optical network availability and/or to reduce the network latency. In particular, the correlation coefficient between popularity and mean cloud probability is -0.446, which, indicates that the higher the mean cloud probability at a location, the less likely it would be a good choice for an OGS. Another interesting observation is that the most popular OGSs are mainly located in the $\pm 20°$ to $\pm 40°$ latitude band, as shown in Figure 10 (right) and Figure 7. Finally, popularity decreases as cost increases, independent of any other variables (see Figure 10 left). Table 3 summarizes the correlation coefficients between OGS popularity and three aforementioned variables.

Table 3: **Correlation coefficients between popularity and mean cloud probability, latitude, and cost of the OGSs**

	Mean cloud prob.	Latitude	Cost
r with popularity	-0.446	-0.159	-0.333

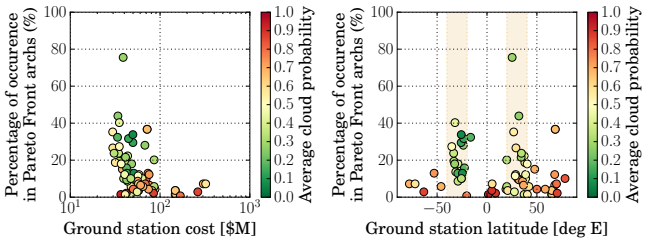

Figure 10: **Percentage of occurrence in the Pareto-front architectures vs. ground station cost and ground station latitude. The marker color indicates the average cloud probability ($\bar{\theta}_c$) across the analysis timespan. The shaded region on the right image corresponds to the $\pm 20°$ to $\pm 40°$ latitude band.**

We conclude this analysis by studying the difference in terms of network availability between the optical scenario and the RF scenario, to quantify the effect of link outages due to cloud coverage in the availability of the networks. For the optical system to be attractive, the achievable data rate must be higher or equal than the inverse of the ratio between the RF network availability and the ONA (such that the data volume downloaded using optical technology is greater or equal than the data volume achieved using RF technology).

Figure 11 shows the ratio between the network availability obtained when using RF technology (NA_{RF}), assuming an identical minimum elevation angle of 20 degrees, and the availability achieved when using optical technology, (ONA), as well as the increase in data rate required when using

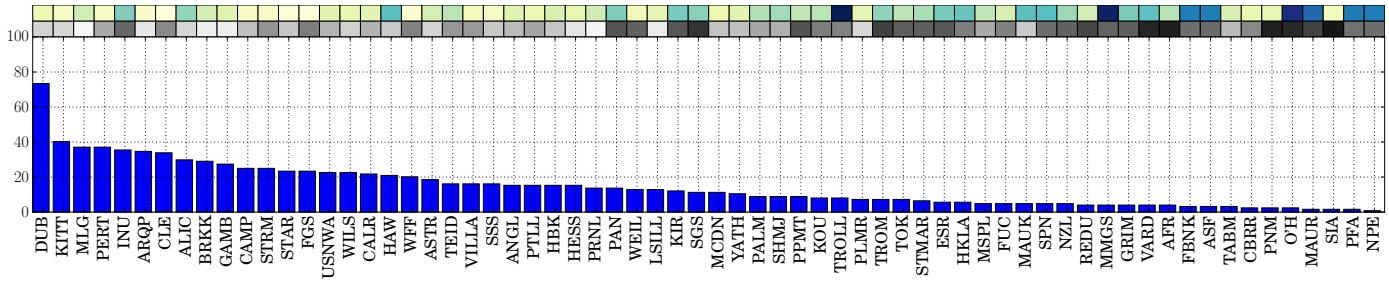

Figure 9: **Percentage of occurrence of each ground station in the Pareto-front architectures for the Fixed candidate set scenario. The first top row of colored squares is a measure of the relative cost between ground station (blue = high cost, yellow = low cost), while the second row of colored squares represents the mean cloud probability of the OGS (dark = clouded skies, white = clear skies). The full list of ground stations can be found in Table 4**

optical technology to match the data volumes returned by RF systems. For example, if the ratio ONA/NA$_{RF}$ is 0.5, (the availability achieved by the network is half of the availability when using RF), the data rate of the optical terminal must be at least twice of the RF subsystem in order to achieve greater or equal performance. We observe that for the Pareto-front architectures, the ratio between availabilities is between 0.5 and 0.8, which in turn results in data rates 1.3 - 2 times higher than the data rates of RF technology. In contrast, for the general case, the ratio between availabilities values ranges from 0.4 to 0.7 and between 1.4 - 2.5 for the increase in data-rate factor. Note that for both types of architectures, the increase in data-rate values are easily attainable as optical technology can deliver data-rates 10-100 times higher than current technology.

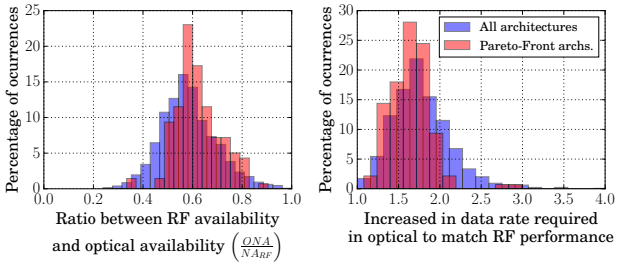

Figure 11: **Ratio between network availabilities when using RF technology and optical technology (left), and increase in data rate required to match performance of RF when using optical technology (right).**

Unconstrained scenario

In this analysis, we look for the optimal locations for a network of OGSs that serve LEO satellite missions, considering as a candidate location every point on the Earth (excluding countries that are banned due to political instability reasons, as explained in Section 3). We use the same assumptions as in the previous subsection for the user-base and timespan of the analysis, and use the same methodology to compute the latency and monthly availability (described in Section 2). We configure out VLC-GA with the following parameter set-up: N = 200,000 , $R_{top} = 10\%$, $R_{bottom} = 10\%$, and R = 8000. (See [27] for a complete explanation of these parameters).

Figure 13 shows the resulting tradespace for this analysis. In this case, the maximum ONA reported is 8.85 %, whereas the minimum latency is 3 hours and 15 minutes. The same trends to those described for the fixed scenario can be identified in this tradespace.

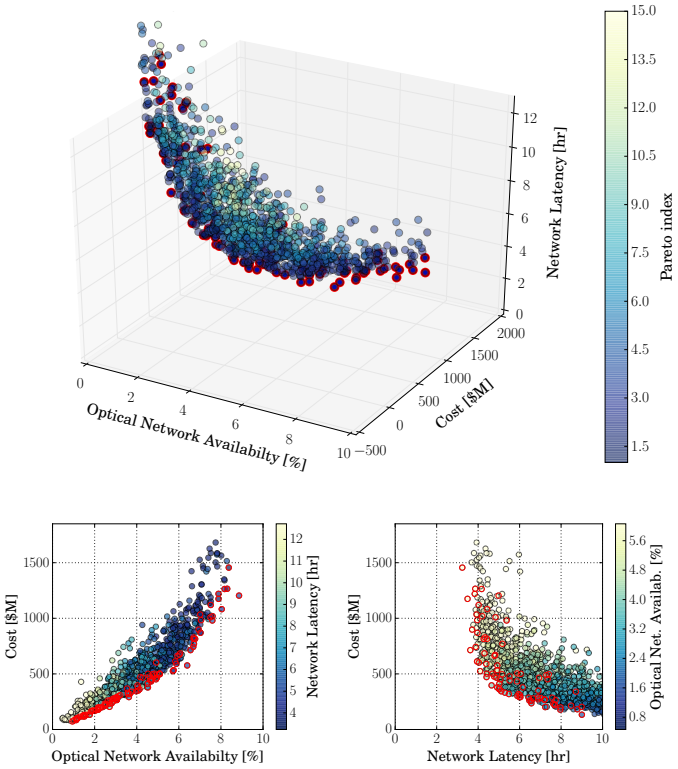

Figure 13: **Tradespace results for the Fixed candidate set scenario. Each marker represents an architecture. The metric-space is represented in the top graph, whereas projections of this space in the ONA-cost (left) and latency-cost (right) are represented in the bottom views. Architectures in the Pareto-front are marked in red.**

Figure 12 shows a heatmap of the popularity of different regions of the world. This popularity is computed using the Pareto-index metric of the region where each latitude-longitude point falls in (the regions are determined using the VLC-GA algorithm ax explained in Section 4). These results show again that the $\pm 20°$ to $\pm 40°$ latitude bands contain the

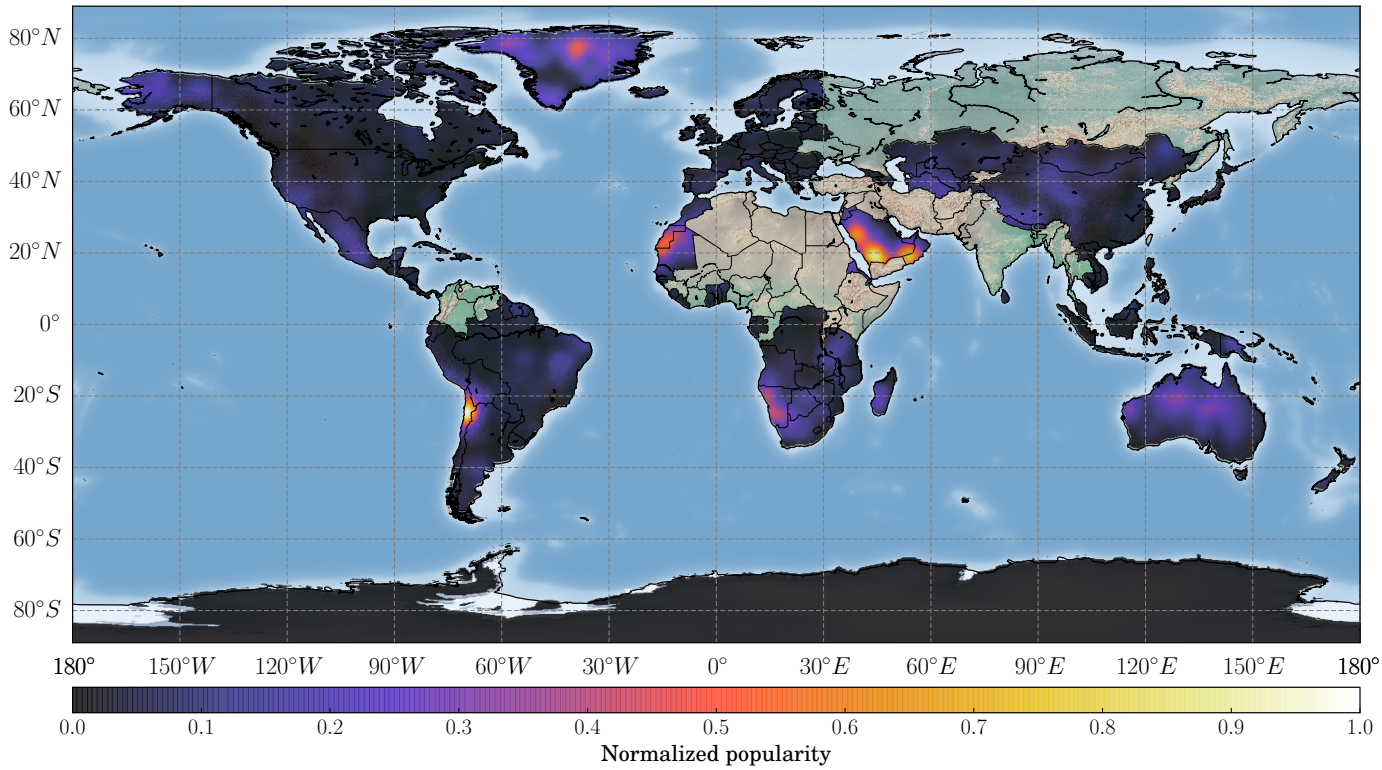

Figure 12: **World-map view of the popularity of the OGSs for the unconstrained scenario. The popularity of each point is computed using the Pareto-index metric of every region (see Section 4 and reference).**

most popular options. In addition to some of the locations previously identified (e.g., The Andes region Namibia and Australia), new locations appear on the heatmap with high intensity. These include the south of Saudi Arabia, the north of Mexico, the Saharan region, and the center of Greenland. Note that even though intuition might lead us to think that the enormous maintenance and operations cost for the Sahara and Greenland regions would make them unpopular locations, our models categorize them as important options to consider. We believe that this might be due to the infrastructure model failing to provide good cost estimates for the harsh-environment regions of the world. Further validation of the cost model is needed to confirm these findings.

6. Conclusions

The optimal location of optical ground stations that serve LEO missions is shown. Three performance-metrics are considered during the optimization process: network availability, latency between successive contacts, and the cost of the network. A simple stochastic weather generator was developed to generate cloud occurrence sequences, which in turn are used to compute the values of the network availability and the latency, while the cost model introduced in [14] was used to obtain an estimate of the cost. The stochastic weather generator only needs as its inputs the monthly cloud probabilities on each OGS, which are obtained form the data registered by the MODIS instruments of satellites TERRA and AQUA in the last 15 years. The cost model uses as inputs the distance to the closest WAN access-point, as well as the construction and maintenance and operations costs, described in the DoD Facilities Pricing Guide [24].

Two case studies were conducted using these models: in the first , a fixed candidate set of OGS is considered. This set is composed of existing facilities that belong to international agencies (NASA, ESA) and to commercial ground-segment service providers (KSAT, SSC); in the second, the ground stations can be located in any latitude-longitude combination on Earth.

Results for the fixed candidate set scenario show that the main variable to determine the optimal locations of the OGSs is cloud probability at that location, which results in new architectures where polar-latitude facilities are no longer attractive assets, since they suffer from high cloud probabilities during all months of the year. Instead, OGSs located in the 20° - 40° latitude band in both hemispheres are deemed as the most attractive locations. We also observed that the increase in cost required to reduce the latency below 5 hours is very high. Finally, as long as optical technologies deliver data-rates more than 3 times higher than RF technology, transitioning to optical systems would enable the customer missions to download a higher data volume.

Results for the unconstrained scenario confirm that the 20° to 40° latitude band contains most of the optimal locations, and reveal new locations where no facilities exist at the moment, which might be interesting options for future new ground stations. These new locations include Saudi Arabia, the North of Mexico, and surprisingly, the Sahara region and the center of Greenland. Further validation of the cost model would be needed to confirm the latter two options as actually promising locations.

Future Work

Several areas of work in this paper would benefit from further research. The Markov chain-based stochastic weather generator model could be further improved so that the cloud occurrence sequences generated have higher resemblance to the real dynamics of cloud cover. There are two areas of improvement in this direction. First, by adding extra parameters in addition to the mean cloud probability (θ_c) for each OGS, and using more complex models such as Hidden Markov Models, or region-based models as those described in [31], the fidelity of the model can be increased (i.e., make the PDF of the resulting cloud occurrence sequence more similar to the experimental PDFs). Second, the Markov model should be expanded so that more than two spatially-correlated sites scenarios can be modeled (i.e., networks where 3 or more OGSs are geographically close located can be analyzed).

Furthermore, from an analysis perspective, it would be interesting to study one scenario where the spacecraft carry hybrid communication subsystems that include both optical and RF payloads. Such analysis may verify the results of this paper (that polar-latitude facilities are not as attractive as they are in RF-networks, due to high cloud probabilities) also hold for hybrid systems. These studies would help decision-makers better understand the trade-offs between increases in availability, reduced latency, and costs of hybrid RF-optical vs. optical-only networks. Finally, our infrastructure model needs further validation to confirm that some of the new locations our study found as interesting options are indeed promising locations. This will help designers choose locations for new ground stations need to be built in the future.

APPENDIX

Table 5: **Acronyms**

CER	Cost Estimating Relationship
CDF	Cumulative Distribution Function
DoD	Department of Defense
ESA	European Space Agency
EO	Earth Observation
EDRS	European Data Relay System
FSO	Free Space Optics
FY	Fiscal year
GA	Genetic Algorithm
GEO	Geosynchronous Orbit
GOES	Geostationary Operational Environmental Satellite
HEO	High Elliptical Orbit
IXP	Internet eXchange Point
ISCCP	International Satellite Cloud Climatology Project
KSAT	Kongsberg Satellite Services
lat_m	Monthly Latency
LEO	Low Earth Orbit
LNOT	Lasercom Network Optimization Tool
LOS	Line of Sight
MODIS	Moderate Resolution Imaging Spectroradiometer
MTSAT	Multi-Functional Transport Satellite
NA_m	Monthly Network Availability
NASA	National Aeronautics and Space Administration
NEN	Near Earth Network
NOAA	National Oceanic and Atmospheric Administration
NSGA-II	Non-Dominated Sorting Genetic Algorithm - II
OGS	Optical Ground Station
ONA	Optical Network Availability
PDF	Probability Density Function
RF	Radio-frequency
SSC	Swedish Space Corporation
SSO	Sun-Synchronous Orbit
STK	Systems ToolKit
TDRSS	Tracking and Data Relay Satellite System
VLC-GA	Variable Length Chromosome Genetic Algorithm
WAN	Wide Area Network

ACKNOWLEDGMENTS

The authors would like to thank the *Fundación Obra Social de La Caixa* for partially funding this project.

Table 4: **List of candidate optical ground stations for the fixed-candidate set scenario**

ID	Name	Code	Latitude	Longitude	Altitude	Country	Category
1	Alaska Satellite Facility	ASF	64.86	-147.85	0	USA	NEN (NASA)
2	Clewiston	CLE	26.73	-82.03	3	USA	SSC
3	Esrange	ESR	67.88	21.07	341	Sweden	SSC
4	Florida Ground Station	FGS	29.00	-81.00	0	USA	NEN (NASA)
5	Fucino	FUC	42.00	13.55	652	Italy	SSC
6	Hartebeesthoek	HBK	-25.64	28.08	1288	South Africa	SSC
7	Inuvik	INU	68.40	-133.5	51	Canada	SSC
8	McMurdo Ground Station	MMGS	-77.81	166.69	183	Antartica	NEN (NASA)
9	North Pole	NPE	64.80	-147.5	145	USA	SSC
10	O'Higgins	O'H	-63.32	-57.9	26	Antartica	SSC
11	Poker Flat	PFA	65.12	-148.45	0	USA	NEN (NASA)
12	Punta Arenas	PAN	-53.00	-71.00	88	Argentina	SSC
13	Santiago Satellite Station	SSS	-33.13	-70.67	698	Chile	SSC
14	South Point	SPN	19.00	-155.6	164	USA	SSC
15	Svalbard Ground Station	SGS	78.22	15.39	248	Norway	NEN (NASA)
16	USN Western Australia	USNWA	-29.05	114.9	24	Australia	SSC
17	Wallops Flight Facility Ground Stations	WFF	37.94	-75.49	11	USA	NEN (NASA)
18	Weilheim	WEIL	47.84	11.14	561	Germany	SSC
19	Yatharagga	YATH	-29.05	115.35	280	Australia	SSC
20	AliceSprings	ALIC	-23.7	133.88	581	Australia	Observatories
21	AngloAust	ANGL	-31.28	149.07	1135	Australia	Observatories
22	Arequipa	ARQP	-16.41	-71.54	2321	Peru	Observatories
23	Astron	ASTR	-32.38	20.81	1737	South Africa	Observatories
24	Brukkaros	BRKK	-25.88	17.78	945	Namibia	Observatories
25	Calar Alto	CALR	37.22	-2.55	2157	Spain	Observatories
26	Gamsberg	GAMB	-23.33	16.33	1781	Namibia	Observatories
27	HESS	HESS	-22.61	17.06	1706	Namibia	Observatories
28	Kitt Peak	KITT	31.96	-111.6	1991	USA	Observatories
29	La Palma	PALM	28.71	-17.91	1006	Spain	Observatories
30	Las Campanas	CAMP	-33.42	-70.56	688	Chile	Observatories
31	La Silla	LSILL	-29.26	-70.74	2332	Chile	Observatories
32	Mauna Kea	MAUK	19.82	-155.47	4184	USA	Observatories
33	McDonald	MCDN	30.67	-104.02	2001	USA	Observatories
34	Haleakala	HKLA	20.72	-156.26	2109	USA	Observatories
35	Stromlo	STRM	-35.32	149.01	779	Australia	Observatories
36	Wilson	WILS	34.23	-118.07	1728	USA	Observatories
37	Palomar	PLMR	33.36	-116.84	1780	USA	Observatories
38	Paranal	PRNL	-24.63	-70.40	2065	Chile	Observatories
39	Perth	PERT	-32.07	115.83	25	Australia	Observatories
40	Purple Mountain	PPMT	32.07	118.83	159	China	Observatories
41	Shokin Majdanak	SHMJ	38.72	66.88	2228	Uzbekistan	Observatories
42	Starfire	STAR	34.52	-105.87	1950	USA	Observatories
43	Table Mountain	TABM	37.19	-118.58	2719	USA	Observatories
44	Teide	TEID	28.27	-16.64	2340	Spain	Observatories
45	Fairbanks	FBNK	64.80	-147.70	135	USA	KSAT
46	Inuvik	INU	68.40	-133.5	51	Canada	KSAT
47	Hawaii	HAW	19.82	-155.47	4184	USA	KSAT
48	Tokyo	TOK	35.69	139.69	37	Japan	KSAT
49	Singapore	SIA	1.35	103.82	55	Singapore	KSAT
50	Trollsat	TROLL	-72.10	2.32	1270	Antartica	KSAT
51	Vardo	VARD	70.37	31.1	1	Norway	KSAT
52	Tromso	TROM	69.65	18.96	4	Norway	KSAT
53	Grimstad	GRIM	58.34	8.59	28	Norway	KSAT
54	Puertollano	PTLL	38.69	-4.11	703	Spain	KSAT
55	Dubai	DUB	25.2	55.27	0	UAE	KSAT
56	Mauritius	MAUR	-20.35	57.55	579	Mauritius	KSAT
57	Panama	PNM	8.54	-80.78	1057	Panama	KSAT
58	Hartebeesthoek	HBK	-25.64	28.08	1288	South Africa	KSAT
59	Central Africa	AFR	4.84	10.10	205	Central Africa	KSAT
60	New Zeland	NZL	-46.02	167.81	120	New Zeland	KSAT
61	Kourou	KOU	5.16	-52.65	15	French Guiana	ESA
62	Kiruna	KIR	67.86	20.23	402	Sweden	ESA
63	Redu	REDU	50.00	5.16	386	Belgium	ESA
64	Cebreros	CBRR	40.46	4.46	794	Spain	ESA
65	Villafranca	VILLA	40.26	-3.57	664	Spain	ESA
66	Maspalomas	MSPL	27.45	-15.38	205	Spain	ESA
67	Santa Maria	STMAR	36.59	-25.08	276	Portugal	ESA
68	Malargue	MLG	-25.78	-69.40	1550	Argentina	ESA

REFERENCES

[1] M. Sanchez, I. del Portillo, E. Crawley, and B. Cameron, "Approximation methods for estimating the availability of optical ground networks," *Journal of Optical Communications and Networking*, vol. 8, no. 10, pp. 800–812, 2016.

[2] C. Fuchs and F. Moll, "Ground station network optimization for space-to-ground optical communication links," *Optical Communications and Networking, IEEE/OSA Journal of*, vol. 7, no. 12, pp. 1148–1159, 2015.

[3] S. Poulenard, M. Crosnier, and A. Rissons, "Ground segment design for broadband geostationary satellite with optical feeder link," *Journal of Optical Communications and Networking*, vol. 7, no. 4, pp. 325–336, 2015.

[4] K.-J. Schulz, J. Rush, and et. al., "Optical link study group final report," Interagency Operations Advisory Group, Tech. Rep., 2012.

[5] EUMETSAT, "MSG Ground Segment LRIT/HRIT Mission Specific Implementation," p. 21, 2015.

[6] S. Poulenard, M. Ruellan, B. Roy, J. Riédi, F. Parol, and A. Rissons, "High altitude clouds impacts on the design of optical feeder link and optical ground station network for future broadband satellite services," in *SPIE LASE*. International Society for Optics and Photonics, 2014, pp. 897 107–897 107.

[7] G. S. Wojcik, H. L. Szymczak, R. J. Alliss, R. P. Link, M. E. Craddock, and M. L. Mason, "Deep-space to ground laser communications in a cloudy world," in *Optics & Photonics 2005*. International Society for Optics and Photonics, 2005, pp. 589 203–589 203.

[8] F. Lacoste, A. Guérin, A. Laurens, G. Azema, C. Périard, and D. Grimal, "Fso ground network optimization and analysis considering the influence of clouds," in *Antennas and Propagation (EUCAP), Proceedings of the 5th European Conference on*. IEEE, 2011, pp. 2746–2750.

[9] Y. Takayama, M. Toyoshima, and N. Kura, "Estimation of accessible probability in a low earth orbit satellite to ground laser communications," *Radioengineering*, vol. 19, no. 2, pp. 249–253, 2010.

[10] T. Jono, Y. Takayama, N. Kura, K. Ohinata, Y. Koyama, K. Shiratama, Z. Sodnik, B. Demelenne, A. Bird, and K. Arai, "Oicets on-orbit laser communication experiments," in *Lasers and Applications in Science and Engineering*. International Society for Optics and Photonics, 2006, pp. 610 503–610 503.

[11] D. Giggenbach, F. Moll, C. Fuchs, and M. Brechtelsbauer, "Direct optical high speed downlinks and ground station networks for small LEO missions," in *16th Ka-and Broadband communications conference*, 2010.

[12] W. B. Rossow and R. A. Schiffer, "ISCCP cloud data products," *Bulletin of the American Meteorological Society*, vol. 72, no. 1, pp. 2–20, 1991.

[13] D. S. Wilks and R. L. Wilby, "The weather generation game: a review of stochastic weather models," *Progress in Physical Geography*, vol. 23, no. 3, pp. 329–357, 1999.

[14] I. del Portillo, M. Sanchez, B. G. Cameron, E. F. Crawley, and D. Selva, "Architecting the ground segment of an optical space communication network," in *2016 IEEE Aerospace Conference*, 2016.

[15] L. Clare and G. Miles, "Deep space optical link arq performance analysis," in *2016 IEEE Aerospace Conference*, March 2016, pp. 1–11.

[16] E. N. Gilbert, "Capacity of a burst-noise channel," *Bell system technical journal*, vol. 39, no. 5, pp. 1253–1265, 1960.

[17] J. Simpson, "Use of the gamma distribution in single-cloud rainfall analysis," *Monthly Weather Review*, vol. 100, no. 4, pp. 309–312, 1972.

[18] E. Chia and M. Hutchinson, "The beta distribution as a probability model for daily cloud duration," *Agricultural and forest meteorology*, vol. 56, no. 3, pp. 195–208, 1991.

[19] G. Rubino and B. Sericola, "Sojourn times in finite markov processes," *Journal of Applied Probability*, pp. 744–756, 1989.

[20] Platnick, S., Ackerman, S., King, M., et al., "MODIS Atmosphere L2 Cloud Product (06L2)," *NASA MODIS Adaptive Processing System, Goddard Space Flight Center*, 2015.

[21] P. Garcia, A. Benarroch, and J. M. Riera, "Spatial distribution of cloud cover," *International Journal of Satellite Communications and Networking*, vol. 26, no. 2, pp. 141–155, 2008.

[22] P. Y. Bely, "Large space optics," in *Next Generation Space Telescope Science and Technology*, vol. 207, 2000, p. 25.

[23] L. M. Stepp, L. G. Daggert, and P. E. Gillett, "Estimating the cost of extremely large telescopes," in *Astronomical Telescopes and Instrumentation*. International Society for Optics and Photonics, 2003, pp. 309–321.

[24] Department of Defense. (2015) The DoD Facilities Pricing Guide.

[25] A. Graphics, "Inc (agi) systems tool kit (stk)," *AGI Product Literature*, 2014.

[26] The Worldwide Governance Indicators (WGI) project, The World Bank Group, "Political Stability and Absence of Violence/Terrorism," viewed 10th August, 2016, http://data.worldbank.org/data-catalog/worldwide-governance-indicators.

[27] I. del Portillo, "Optimal locations for the ground segment of optical space communications networks," Master's thesis, Massachusetts Institute of Technology Department of Aeronautics and Astronautics, Cambridge, Massachusetts, June 2016.

[28] K. Deb, A. Pratap, S. Agarwal, and T. Meyarivan, "A fast and elitist multiobjective genetic algorithm: NSGA-II," *Evolutionary Computation, IEEE Transactions on*, vol. 6, no. 2, pp. 182–197, 2002.

[29] R. Poli, J. E. Rowe, C. R. Stephens, and A. H. Wright, "Allele diffusion in linear genetic programming and variable-length genetic algorithms with subtree crossover," in *European Conference on Genetic Programming*. Springer, 2002, pp. 212–227.

[30] G. Syswerda, "Uniform crossover in genetic algorithms," 1989.

[31] P. Ailliot, D. Allard, V. Monbet, and P. Naveau, "Stochastic weather generators: an overview of weather

type models," *Journal de la Société Française de Statistique*, vol. 156, no. 1, pp. 101–113, 2015.

BIOGRAPHY

Iñigo del Portillo *is a Ph.D. candidate in the department of Aeronautics and Astronautics at MIT. His research interests include system architecture for space-based networks, space optical communications systems, and small satellites communications. Iñigo received his degrees in Industrial Engineering, Electronics Engineering and Telecommunications Engineering in 2014 from Universitat Politecnica de Catalunya, Barcelona, and his M.Sc. in aeronautics and astronautics from MIT in 2016.*

Marc Sanchez Net *is currently a fourth year Ph.D. candidate in the department of Aeronautics and Astronautics at MIT. His research focuses on architecting space communication networks to support future space exploration activities. He has interned twice at NASAs Jet Propulsion Laboratory in the Communication Architecture and Research Section. He received his M.S. in aeronautics and astronautics in 2014 from MIT, and also holds degrees in both telecommunications engineering and industrial engineering from Universitat Politecnica de Catalunya, Barcelona.*

Dr. Bruce Cameron *is a Lecturer in Engineering Systems at MIT and a consultant on platform strategies. At MIT, Dr. Cameron ran the MIT Commonality study, a 16 firm investigation of platforming returns. Dr. Cameron's current clients include Fortune 500 firms in high tech, aerospace, transportation, and consumer goods. Prior to MIT, Bruce worked as an engagement manager at a management consultancy and as a system engineer at MDA Space Systems, and has built hardware currently in orbit. Dr. Cameron received his undergraduate degree from the University of Toronto, and graduate degrees from MIT.*

Dr. Edward F. Crawley *received an Sc.D. in Aerospace Structures from MIT in 1981. His early research interests centered on structural dynamics, aeroelasticity, and the development of actively controlled and intelligent structures. Recently, Dr. Crawleys research has focused on the domain of the architecture and design of complex systems. From 1996 to 2003 he served as the Department Head of Aeronautics and Astronautics at MIT, leading the strategic realignment of the department. Dr. Crawley is a Fellow of the AIAA and the Royal Aeronautical Society (UK), and is a member of three national academies of engineering. He is the author of numerous journal publications in the AIAA Journal, the ASME Journal, the Journal of Composite Materials, and Acta Astronautica. He received the NASA Public Service Medal. Recently, Prof Crawley was one of the ten members of the presidential committee led by Norman Augustine to study the future of human spaceflight in the US.*